Manufacturing Letters xxx (xxxx) xxx

Contents lists available at ScienceDirect

Manufacturing Letters

journal homepage: www.elsevier.com/locate/mfglet

Electrochemical additive manufacturing of graded NiCoFeCu structures for electromagnetic applications

Anne Brant, Murali Sundaram *

Department of Mechanical and Materials Engineering, University of Cincinnati, Cincinnati, OH 45220, USA

A R T I C L E I N F O

Article history:
Received 14 April 2021
Received in revised form 1 June 2021
Accepted 7 June 2021
Available online xxxx

Keywords:
Electroforming
Graded electrodeposition
Micro additive manufacturing

A B S T R A C T

This study introduces the concept of compositionally-graded electrochemical additive manufacturing of advanced metal alloys. The feasibility was demonstrated using a NiCoFeCu system for electromagnetic applications. The effects of grading frequency and voltage on output geometry and elemental composition were studied. Application of constant signals throughout pillar build yielded varying width and elemental composition along the pillar length. Additional grading of voltage from low to high favoured wider pillars and enhanced copper content. Auxiliary plating effects were used to explain compositional deviations from conventional electroplating. Frequency response varied with voltage, suggesting its use as a secondary, fine-tuned parameter.

1. Introduction

Interest in metal alloys of varying compositions, and assemblies of such components, is on the rise across many applications where a balance of functionality (i.e.: electromagnetic), constraints (i.e.: weight), and resistance to elements (i.e.: thermal, corrosion, wear) is desired [1]. However, methods of composite assembly introduce design constraints and manufacturing complexity [2]. An alternative to fabricate such parts is functionally-graded additive manufacturing (FGAM), in which multi-material additive manufacturing is performed using spatially-varying compositions of metals [3] via discrete, computerized control [4]. However conventional FGAM of metals relies on metallurgical (thermomechanical) means of alloy formation, presenting serious issues in process control and integrity of the final part. Due to these complications, metal FGAM processes remain in a technologically early state [1]. Electrochemical additive manufacturing (ECAM) is emerging as an alternate, nonthermal means of additive manufacturing (AM) [5]. Electrochemical deposition of metals involves an entirely different crystallization mechanism than that of thermal processes. Electrochemical deposition allows for more-dispersed alloys (ie: solid solutions for a silver-lead system) to be deposited; in contrast to metallurgy, which is limited to production of eutectic mixtures [6].

Although a variety of systems and parameters have been studied for ECAM, the concept of compositionally-graded ECAM-built parts has not yet been performed [7] and is therefore the focus of this study and termed CG-ECAM. In this study, a combination of elements relevant to electromagnetic applications is deposited, consisting of: (1) magnetic regions with relatively higher amounts of iron-group metals nickel, cobalt, and iron; versus (2) conductive regions with a relatively higher percentage of copper. Together, the ability of ECAM to localize deposits [5], along with the control over composition and microstructure in metal electrodeposition [8–10], make CG-ECAM a promising manufacturing process to fabricate parts for such applications.

2. Method

An in-house-built experimental setup combining microcontrollers (Arduino Mega and Adafruit v2 Motorshields), positioning hardware (three-axis stage of Zaber LSA-10A stepper motors), potentiostat (hand-built), and electrochemical cell (0.25 mm Pt-Ir wire tool and brass plate substrate). The system and voxel-by-voxel closed-loop control deposition method resembled that of prior work [5] with the additional capability of changing deposition conditions in a voxel-by-voxel manner and the use of a multi-metal plating bath (0.5 M $NiSO_4{\cdot}6H_2O$, 0.1 M $CoSO_4{\cdot}7H_2O$, 0.01 M $FeCl_2{\cdot}4H_2O$, 0.05 M $CuSO_4{\cdot}5H_2O$, 0.485 M H_3BO_3, 0.5 M $Na_3Cit{\cdot}2H_2O$, 0.1 mM PEG_{3350}, and 0.18 mM H_2SO_4.) The voxel size was defined to be 3 motor steps (4.5 μm), and vertical pillars of 300 voxel height (totaling 1350 μm) were constructed using a pulsed square wave of constant or varying voltage and/or frequency. The duty cycle was kept constant at 50%.

A parameter space of low and high tool-substrate voltage differences (V_{low} = 4.5 and V_{high} = 5.5 V) and frequencies (f_{low} = 100 and f_{high} = 1000 Hz) was used in this study. Pillars were initially

* Corresponding author.

https://doi.org/10.1016/j.mfglet.2021.06.003

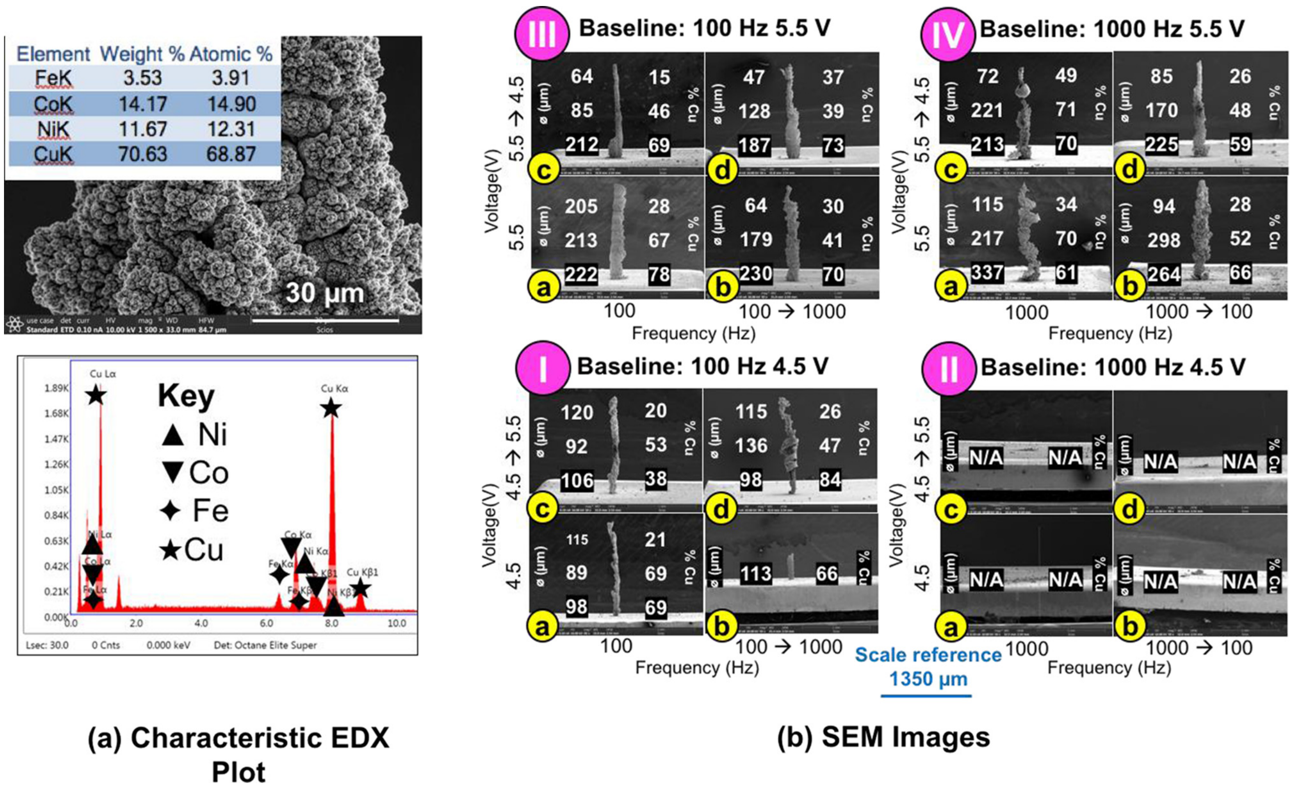

Fig. 1. Pillar characterization: (a) Representative close-up SEM image and EDX scan at the midpoint of pillar built under baseline conditions 4.5 V and 100 Hz, (b) SEM images of compositionally-graded pillars; N/A refers to broken/incomplete deposits.

fabricated under constant-voltage, constant-frequency conditions at all combinations – these "baseline" conditions were then incrementally changed to study the additional effect of grading one or both parameters. Baseline low-level parameters were graded up to the high level and vice-versa. Images and atomic percentage quantities of elements deposited were obtained using scanning electron microscopy (SEM), and energy-dispersive X-ray spectroscopy (EDX). A representative image showing a close-up view of the surface and elemental scan of the deposit is shown in Fig. 1(a).

3. Results and discussion

SEM images of the final pillars are shown in Fig. 1(b). Pillar widths and copper content percentages at 1/3, 2/3, and full pillar height were manually located and resulting values are inset within the figures. The major quadrants (I-IV) correspond to a given baseline frequency and voltage condition. Within each quadrant, varying grading patterns are shown: (a) both parameters ungraded, (b) frequency graded, (c) voltage graded, and (d) both parameters graded. Any changes in copper content are implicitly accompanied by an opposing change in total magnetic element (NiCoFe) content. Statistical analysis was performed to understand main and interaction effects on elemental content of the pillars [11].

3.1. Effect of baseline parameters on output pillar width and composition

Table 1 analyzes the average width and copper content of pillars at all constant baseline signals (runs denoted by subscript a). Width and copper content were both higher when comparing V_{high} versus V_{low} (218 vs 101 µm and 56 vs 53% Cu), but less-significantly impacted when comparing f_{high} versus f_{low} (223 vs

Table 1
Main and interaction effects of baseline signals on average output width (first value in µm) and Cu content (second value in atomic %) in pillars; annotations in the table correspond to trials that were averaged.

Parameter	f_{low}	f_{high}	Main eff.	Int. eff.
V_{low}	101/*53* (Ia)	N/A/*N/A* (IIa)	101/*53*	N/A/*N/A*
V_{high}	213/*57* (IIIa)	223/*55* (IVa)	218/*56*	10/*2*
Main eff.	157/*55*	223/*55*		
Int. eff.	112/*4*	N/A/*N/A*		

157 µm and 55 vs 55% Cu). Interactions could not be compared at V_{low} due to consistent breakage of pillars built under its combination with f_{high} (Quadrant II). Trial Ib (4.5 V, graded 100–1000 Hz) consists of a pillar approaching these conditions in its upper half, which broke off. This suggests that pillars built using V_{low} and f_{high} at the pillar base failed early in the build failed due to a fragile geometry under the bubbling electrolyte beneath the tool. Although higher frequencies would be expected to deposit more copper [12], there was no systematic main effect of frequency on copper content. Overall, the observed behavior elucidates (1) a voltage-dependent frequency response and (2) limited deposition capabilites at specific voltage-frequency combinations.

The higher average copper content seen at a higher voltage appears opposite to what is expected from the electrochemical series. This deviation may be explained by copper ion complexation with citrate, which minimizes its reduction potential relative to iron-group metals [13–16]. Deviation of a similar nature emerged in ECAM of NiCu pillars using a citrate bath [17]. Additionally, the active plating area is not discretely confined to the tool-substrate gap. Instead, it tapers off gradually, exposing the entire substrate and built voxels to relatively low current densities that

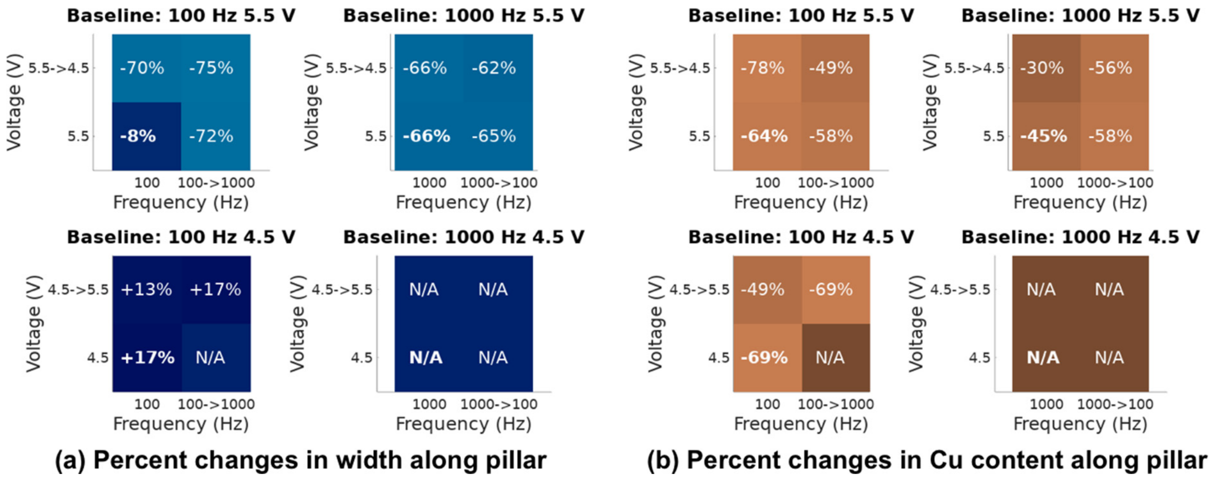

Fig. 2. Percent changes from bottom to top of pillar: (a) width and (b) Cu content.

Table 2
Main and interaction effects of signal grading patterns on graded percent change in output width (first value) and Cu content (second value) along pillar length; annotations in the table correspond to trials that were averaged.

Parameter	f↓	$f_{ungraded}$	f↑	Main eff.	Int. eff.
V↓	−62/*−56* (IVd)	−68/*−54* (IIIc, IVc)	−75/*−49* (IId)	−68/*−53*	6/*24*
$V_{ungraded}$	−65/*−58* (IVb)	−14/*−44* (Ia, IIa, IIIa, IVa)	−72/*−58* (IIIb)	−32/*−49*	55/*22*
V↑	N/A/*N/A* (N/A)	+7/*−25* (Ic, IIc)	+17/*−69* (Id)	+10/*−39*	11/*45*
Main eff.	−63/*−57*	−22/*−42*	−43/*−59*		
Int. Eff.	2/*3*	40/*32*	46/*10*		

influence plating geometry [5,18]. In CG-ECAM, these conditions would cause higher copper content to accumulate on earlier voxels. A higher tool-substrate voltage difference also raised the overall magnitude of the auxiliary low current densities, likely depositing even more copper [19]. This is reflected in the increase in copper content at the bottom pillar location from 69% to 78% when the baseline voltage was increased from 4.5 to 5.5 V respectively at 100 Hz operation.

3.2. Effects of grading voltage and frequency on graded output pillar width and composition

Next, the feasibility of grading the outputs was evaluated, starting from different initial conditions at the base of the pillars. Percent changes in outputs along pillar length are shown in Fig. 2. Table 2 provides main effects and interactions of varying combinations of applied grading patterns (down, ungraded, or up). Graded changes in output occurred even when both voltage and frequency were ungraded. This behavior suggests that each voxel built was also sensitive to the dynamic electrochemical environment and characteristics of previously-deposited voxels.

Reflecting the trend seen in baseline conditions, changing the voltage grading pattern (from down, to ungraded, to up) resulted in a systematic increase in width (−68% to −32% to +10%) and stifled decrease in copper content (−53% to −49% to −39%) along pillar length. A similar change of frequency grading did not yield systematic changes in narrowing (−63%to −22% to −43%) or decrease in copper content (−57% to −42% to −59%) along pillar length. Width was most sensitive to frequency effects at an ungraded voltage. Copper content was most sensitive to frequency effects at a high voltage. Width was most sensitive to voltage interactions when frequency was graded up. Copper content was most sensitive to voltage when frequency was ungraded. Overall, width and elemental composition varied systematically with voltage, but frequency effects were more complex.

4. Conclusions

Extension of ECAM to a process capable of fabricating compositionally-graded micro pillars was demonstrated by controlling the applied plating signal parameters (voltage and frequency) in a voxel-by-voxel manner and analyzing the effect on the graded pillar width and elemental composition. Starting with a higher baseline voltage yielded slightly higher copper content. This ran counter to what would be expected from the electrochemical series, but was explained by the influence of citrate complexation and auxiliary plating effects. A higher baseline frequency yielded no noticeable main effect on copper content. Although higher copper content was expected at higher frequencies, results instead showed an irregular trend and suggest a complex frequency response of the system.

The degree of width and compositional grading along the micro pillars was quantified by calculating their respective percent changes from the bottom to the top of the pillar. Under a steady baseline signal, these outputs already varied along the length of the pillar. Grading voltage up increased the resulting grading up of pillar width and copper content. An overall increase in copper content along the length of the pillar was also seen – this was likely due to auxiliary plating effects skewing voxels earlier in the build to accumulate more copper during the build of subsequent voxels. This effect could be compensated for via a pre-programmed voltage pattern or more precise potentiostatic control of the substrate. Applied frequency changes did not result in a unified trend across all trials, suggesting that this parameter should be secondary to and fine-tuned with respect to the applied voltage.

Declaration of Competing Interest

The authors declare that they have no known competing financial interests or personal relationships that could have appeared to influence the work reported in this paper.

Acknowledgments

This material is based upon work supported by the National Science Foundation Grants CMMI-1955842 and CMMI-1454181. Any opinions, findings, and conclusions or recommendations expressed in this material are those of the author(s) and do not necessarily reflect the views of the National Science Foundation.

References

[1] Reichardt A, Shapiro AA, Otis R, Dillon RP, Borgonia JP, McEnerney BW, et al. Advances in additive manufacturing of metal-based functionally graded materials. Int Mater Rev 2021;66(1):1–29.
[2] Söderberg R, Wärmefjord K, Lindkvist L. Variation simulation of stress during assembly of composite parts. CIRP Ann 2015;64(1):17–20.
[3] Vaneker T, Bernard A, Moroni G, Gibson I, Zhang Y. Design for additive manufacturing: framework and methodology. CIRP Ann 2020;69(2):578–99.
[4] Thompson MK, Moroni G, Vaneker T, Fadel G, Campbell RI, Gibson I, et al. Design for additive manufacturing: trends, opportunities, considerations, and constraints. CIRP Ann 2016;65(2):737–60.
[5] Sundaram MM, Kamaraj AB, Kumar VS. Mask-less electrochemical additive manufacturing: a feasibility study. J Manuf Sci Eng 2015;137(2).
[6] Brenner A. Electrodeposition of alloys: principles and practice. Academic Press; 1963.
[7] Xu J, Ren W, Lian Z, Yu P, Yu H. A review: development of the maskless localized electrochemical deposition technology. Int J Adv Manuf Technol 2020:1–27.
[8] Mehrizi S, Sohi MH, Seyyed Ebrahimi SA. Study of microstructure and magnetic properties of electrodeposited nanocrystalline CoFeNiCu thin films. Surf Coat Technol 2011;205(20):4757–63.
[9] Shakya P, Cox B, Davis D. Giant magnetoresistance and coercivity of electrodeposited multilayered FeCoNi/Cu and CrFeCoNi/Cu. J Magn Magn Mater 2012;324(4):453–9.
[10] Wu JC, Li L, Harrison JC., Candler RN. Micro-to millimeter scale magnetic shielding. In Proc. 2017 19th International Conference on Solid-State Sensors, Actuators and Microsystems (TRANSDUCERS), IEEE, p. 838–41.
[11] Stockburger DW. Multivariate statistics: Concepts, models, and applications. <http://dwstockburger.com/Multibook/mbk.htm>; 2016, 3rd Web Edition, [accessed 2021].
[12] Beltowska-Lehman E, Ozga P, Chassaing E. Pulse electrodeposition of Ni·Cu·Mo alloys. Surf Coat Technol 1996;78(1-3):233–7.
[13] Chassaing E, Vu Quang K, Wiart R. Kinetics of copper electrodeposition in citrate electrolytes. J Appl Electrochem 1986;16(4):591–604.
[14] Chassaing E, Quang KV, Wiart R. Mechanism of copper-nickel alloy electrodeposition. J Appl Electrochem 1987;17(6):1267–80.
[15] Silva FLG, Garcia JR, Cruz VGM, Luna AS, Lago DCB, Senna LF. Response surface analysis to evaluate the influence of deposition parameters on the electrodeposition of Cu–Co alloys in citrate medium. J Appl Electrochem 2008;38(12):1763–9.
[16] Stout LE, Faust CL. Electrodeposition of Iron-copper-nickel alloys: part III: deposition from sulfate-boro-citrate baths. Trans Electrochem Soc 1933;64 (1):271. https://doi.org/10.1149/1.3504526.
[17] Sundaram M, Kamaraj AB, Lillie G. Experimental study of localized electrochemical deposition of Ni-Cu alloy using a moving anode. Procedia CIRP 2018;68:227–31.
[18] Kamaraj A, Lewis S, Sundaram M. Numerical study of localized electrochemical deposition for micro electrochemical additive manufacturing. Procedia CIRP 2016;42:788–92.
[19] Brant AM, Sundaram MM, Kamaraj AB. Finite element simulation of localized electrochemical deposition for maskless electrochemical additive manufacturing. J Manuf Sci Eng 2015;137(1).